

Tunable Ultrafast Dynamics of Antiferromagnetic Vortices in Nanoscale Dots

Ji Zou,¹ Even Thingstad,¹ Se Kwon Kim,² Jelena Klinovaja,¹ and Daniel Loss¹

¹*Department of Physics, University of Basel, Klingelbergstrasse 82, 4056 Basel, Switzerland*

²*Department of Physics, Korea Advanced Institute of Science and Technology, Daejeon 34141, Republic of Korea*

(Dated: April 30, 2024)

Topological vortex textures in magnetic disks have garnered great attention due to their interesting physics and diverse applications. However, up to now, the vortex state has mainly been studied in microsize ferromagnetic disks, which have oscillation frequencies confined to the GHz range. Here, we propose an experimentally feasible *ultrasmall* and *ultrafast* vortex state in an antiferromagnetic nanodot surrounded by a heavy metal, which is further harnessed to construct a highly tunable vortex network. We theoretically demonstrate that, interestingly, the interfacial Dzyaloshinskii-Moriya interaction (iDMI) induced by the heavy metal at the boundary of the dot acts as an effective chemical potential for the vortices in the interior. Mimicking the creation of a superfluid vortex by rotation, we show that a magnetic vortex state can be stabilized by this iDMI. Subjecting the system to an electric current can trigger vortex oscillations via spin-transfer torque, which reside in the THz regime and can be further modulated by external magnetic fields. Furthermore, we show that coherent coupling between vortices in different nanodisks can be achieved via an antiferromagnetic link. Remarkably, this interaction depends on the vortex polarity and topological charge and is also exceptionally tunable through the vortex resonance frequency. This opens up the possibility for controllable interconnected networks of antiferromagnetic vortices. Our proposal therefore introduces a new avenue for developing high-density memory, ultrafast logic devices, and THz signal generators, which are ideal for compact integration into microchips.

Introduction.—A main theme in modern spintronics is investigating the potential of nonlinear topological magnetic textures for innovative approaches in both classical and quantum information storage [1–8], processing [9–17], and transmission [18–25]. A prominent example that has attracted significant attention in the community is the magnetic vortex texture, which is a topological spin configuration occurring in microscale ferromagnetic disks [26, 27]. It offers promising prospects for a broad spectrum of applications, including stable microwave signal generation [28–30], novel magnetic memory storage [31–35], logic devices [36–38], and reservoir and neuromorphic computing [39–41]. Much progress has been made in the control and manipulation of the vortex state, as well as in exploring these diverse applications [31, 42–53]. However, all these studies have been restricted to vortex states in magnetic disks that possess finite net magnetizations. This restriction arises because the only known mechanism that can stabilize vortex configurations in microsize (or sub-microsize) disks is based on the dipolar interaction that requires the finite magnetization, which in turn limits the vortex oscillation frequency to the GHz or sub-GHz regime [28, 54–57]. Additionally, the microscale footprint of these textures not only hinders high-density integration in microchips but also poses challenges for their application in emerging quantum technologies due to the rapid loss of quantum coherence associated with such large textures.

In this work, we provide a different pathway to realize a vortex state by exploiting the interfacial Dzyaloshinskii-Moriya interaction (iDMI) in the system, which allows us to achieve a stable, *ultrafast*, and *ultrasmall* vortex configuration in magnetic disks even without net magne-

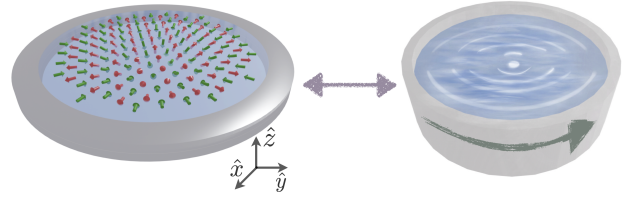


FIG. 1. A schematic of an antiferromagnetic disk (blue) surrounded by a heavy metal (grey) shown in the left panel. The iDMI at the boundary stabilizes vortex configurations in the interior. This is analogous to the formation of a vortex in a superfluid (blue) by rotation shown in the right panel.

tization. We consider an experimentally feasible structure consisting of an antiferromagnetic disk surrounded by a heavy metal, as depicted in the left panel of Fig. 1. In such a structure, the heavy metal provides an iDMI at the boundary of the disk due to the broken inversion symmetry and the strong spin-orbit coupling in the heavy metal [58]. Interestingly, we demonstrate that this interaction acts as an effective chemical potential for vortices in the disk, akin to the rotation of superfluids that is known to induce vortex states. We show that a stable magnetic texture with finite vorticity, exhibiting vortex oscillation frequencies in the THz regime, is achievable in a disk with a diameter of ten nanometers, which would otherwise be impossible due to the dipolar interaction. The vortex state responds to external magnetic fields, which break the time-reversal symmetry, lifting the degeneracy between the left and right circular modes of vortex motion. We further show that electric currents can effectively trigger the ultrafast vortex oscillations exhibit-

ing high quality factors, which thereby serve as stable generators of THz signals.

Exploiting magnetic vortices for unconventional computing and logic operations requires interaction between disks in an interconnected magnetic vortex network [36]. We demonstrate that this is achievable via coherent antiferromagnetic links. Importantly, we find that the coherent interaction, mediated by virtual magnons in the link, depends on both the polarity and topological charge of the two vortices. Furthermore, we demonstrate that this interaction is highly tunable through an applied magnetic field controlling the vortex resonance frequency. Besides offering a nanoscale THz signal generator, our findings also provide opportunities for the development of new types of vortex-based memory and ultra-fast logic devices that combine storage and computation, allowing for high-density integration in microchips due to their nanoscale size.

General idea.—We first discuss how a vortex can emerge as the natural ground state in a magnetic system with vanishing net magnetization. To this end, we consider a thin, easy-plane antiferromagnetic dot of arbitrary shape, surrounded by a heavy metal. The left panel in Fig. 1 shows a circular geometry as an example. The dynamics of the antiferromagnet is described by a smooth Néel vector field $\mathbf{n}(x, y, t)$, which lives on the sphere S^2 for temperatures below the Néel temperature. We introduce another smooth vector field,

$$\mathcal{A}_i = \frac{1}{2\pi} \hat{z} \cdot (\mathbf{n} \times \partial_i \mathbf{n}), \quad (1)$$

which physically describes the *spin winding* of the Néel vector field in the xy -plane (with $i \in \{x, y\}$) [21]. In the limit of strong easy-plane anisotropy such that the Néel vector is confined to the xy -plane, this field \mathcal{A} simplifies to $\mathcal{A}_i = (1/2\pi) \partial_i \phi$, with ϕ being the polar in-plane angle of \mathbf{n} relative to \hat{x} . The *vorticity density* associated with the Néel vector field then can be constructed as

$$\rho_v = \partial_x \mathcal{A}_y - \partial_y \mathcal{A}_x, \quad (2)$$

which is a smooth function for smooth magnetic textures [59]. We remark that, in the xy -plane limit, it reduces to $\rho_v = (1/2\pi) \epsilon^{ij} \partial_i \partial_j \phi$ with the Levi-Civita tensor convention $\epsilon^{xy} = 1$. The vorticity density is therefore zero everywhere except at isolated points with singular vortex cores.

The potential energy governing the energetics of the Néel vector field comprises two parts: The first is the bulk energy $\mathcal{U}_0[\mathbf{n}]$ and the second is the iDMI arising from the strong spin-orbit coupling in the heavy metal and the absence of inversion symmetry at the interface [58, 60–62]. These two parts together give rise to the total energy potential, which can be written into the following form:

$$\mathcal{U}[\mathbf{n}] = \mathcal{U}_0[\mathbf{n}] - 2\pi\mathcal{D} \oint_{\partial\Omega} d\ell \cdot \mathcal{A}, \quad (3)$$

where \mathcal{D} is the iDMI strength and the curve integral is over the boundary $\partial\Omega$ of the magnetic dot. Note that this potential can be rewritten in the more suggestive form $\mathcal{U} = \mathcal{U}_0 - 2\pi\mathcal{D}\mathcal{N}$ by applying Stokes' theorem, where $\mathcal{N} = \int_{\Omega} dx dy \rho_v$ is the total vortex number within the magnetic dot. Thus, the iDMI acts as an *effective chemical potential* for vortices in the antiferromagnetic dot—increasing \mathcal{D} leads to a ground state with finite vorticity.

We remark that this bears close analogy with a rotating superfluid as shown in Fig. 1. In the rotating frame, the superfluid acquires an additional potential term $\sim -\hbar\omega_0\mathcal{N}$ originating from the Coriolis force [63], with rotational frequency ω_0 and total vorticity \mathcal{N} . It is known that the ground state of a superfluid transitions from vortex-free to one with a finite number of vortices above a critical rotational frequency [63]. In our case, the iDMI plays the role of the rotational energy $\hbar\omega_0$. Thus, we conclude that an antiferromagnetic state with finite vorticity forms when the iDMI strength exceeds a critical threshold, $\mathcal{D} > \mathcal{D}_c$. This critical value can be approximately determined by balancing the iDMI and the bulk energy \mathcal{U}_0 associated with a vortex configuration. While it is a non-universal parameter depending on the energetic and geometric details of the magnet, we expect \mathcal{D}_c to be proportional to the magnetic exchange coupling which usually dominates the energy of nonlinear magnetic textures.

Model.—To illustrate the sketched mechanism, we consider a thin easy-plane antiferromagnetic circular dot for concreteness, as shown in Fig. 1, with microscopic Hamiltonian $H = J \sum_{\langle i,j \rangle} \mathbf{S}_i \cdot \mathbf{S}_j + K \sum_i (\mathbf{S}_i \cdot \hat{z})^2$. Here $J > 0$ stands for the antiferromagnetic exchange coupling between two nearest sites $\langle i, j \rangle$, and $K > 0$ defines the hard \hat{z} -axis. The low-energy dynamics of the system is captured by the Néel vector field \mathbf{n} with the effective Lagrangian $\mathcal{L}[\mathbf{n}] = \int dx dy \varrho \dot{\mathbf{n}}^2/2 - \mathcal{U}_0[\mathbf{n}]$, where $\varrho = \hbar t_z/(2Jza^3)$ is the effective inertia with lattice spacing a , the thickness in the \hat{z} -direction t_z , and the coordination number z . The potential energy is

$$\mathcal{U}_0[\mathbf{n}] = \int dx dy \left[\frac{\mathcal{J}}{2} (\nabla \mathbf{n})^2 + \frac{\mathcal{K}}{2} (\mathbf{n} \cdot \hat{z})^2 \right]. \quad (4)$$

Here, the exchange stiffness $\mathcal{J} = JS^2 t_z/a$ and the hard \hat{z} -axis anisotropy $\mathcal{K} = KS^2/a^2$ (with spin length S) penalize states with non-uniform spatial textures and states with \mathbf{n} deviating from the xy -plane, respectively. Together, they define a characteristic length scale $\lambda_0 = \sqrt{\mathcal{J}/\mathcal{K}}$ for the size of vortices in the dot. We consider an antiferromagnetic disk with radius comparable to the vortex size, $R \approx \lambda_0$ [64]. To leverage the circular symmetry of the system, we use polar coordinates (r, φ) , and further adopt the convenient parametrization $\mathbf{n}(r, \varphi) = (\sin \theta \cos \phi, \sin \theta \sin \phi, \cos \theta)$ for the spin texture.

We now wish to examine whether the system favors a ground state with finite vorticity. To this end, we employ the ansatz [65] $\theta = 2 \arctan(r/\lambda_0)$ for $r < \lambda_0$ (otherwise $\theta = \pi/2$) and $\phi = \mathcal{N}\varphi$, which gives a profile with positive polarity $p \equiv n_z(r=0) = +1$ and vortex number \mathcal{N} . This yields a total energy of $\mathcal{U} \propto \mathcal{J}\mathcal{N}^2 - 2\mathcal{D}\mathcal{N}$ [66]. Thus, in the presence of the sizable iDMI (comparable to \mathcal{J}), the system ground state changes from a vortex-free configuration to one with finite vorticity. Considering a NiO antiferromagnetic dot with a thickness of $t_z = 2$ nm, the exchange stiffness is approximately $\mathcal{J} \approx 10^{-21}$ J [67]. The interfacial DM interaction is about $\mathcal{D} \approx 4 \times 10^{-21}$ J $> \mathcal{J}$ for typical heavy metals such as W or Pt (assuming a penetration depth of 2 nm) [60]. With the hard \hat{z} -axis anisotropy being $\mathcal{K} \approx 4.5 \times 10^{-5}$ J/m² [68], the characteristic vortex size (or the radius of the magnetic dot) is evaluated to be around 5 nm. Therefore, an antiferromagnetic vortex state is experimentally feasible in a thin nanoscale magnetic dot.

One important parameter of the system is the characteristic frequency associated with the vortex oscillation in the dot. We consider a configuration $\mathbf{n}(\mathbf{r}, t) = \mathbf{n}_0(\mathbf{r} - \mathcal{R})$ with \mathbf{n}_0 being the previous ansatz with $\mathcal{N} = 1$. Here, $\mathcal{R}(t)$ describes the time-dependent vortex position, and the associated mass $\mathcal{M} \equiv 2\pi\rho$ follows from the Lagrangian for the Néel vector field through $\int d\mathbf{r} \rho \dot{\mathbf{n}}^2/2 = \mathcal{M}\dot{\mathcal{R}}^2/2$. The response of the vortex to a small displacement can be determined by varying the potential energy with respect to \mathcal{R} . The variation of the bulk potential leads to an inverted harmonic potential $\delta\mathcal{U}_0 \approx -\pi\mathcal{J}(\mathcal{R}/\lambda_0)^2$, indicating interactions within the dot disfavor the vortex, pushing it out of the system. Remarkably, the variation of the iDMI generates a harmonic trap $\pi\mathcal{D}(\mathcal{R}/\lambda_0)^2$ for the vortex, effectively retaining it within the system. When the iDMI falls below the critical value $\mathcal{D}_c \equiv \mathcal{J}$, the vortex at the origin would escape from the dot even under a small perturbation. The total vortex potential energy is given by

$$\delta\mathcal{U} \approx \frac{1}{2}\mathcal{M}\Omega_0^2\mathcal{R}^2, \quad \text{with} \quad \Omega_0^2 = \frac{2\pi(\mathcal{D} - \mathcal{D}_c)}{\mathcal{M}\lambda_0^2}. \quad (5)$$

This vortex oscillation frequency is estimated to be about $\Omega_0 = 2\pi \times 0.26$ THz for NiO, which is several orders of magnitude larger than the existing ferromagnetic vortex oscillation frequency.

Magnetic field and spin-transfer torque.—Magnetic fields and electric currents stand out as the most effective tools for manipulating magnetic states in modern spintronics [69, 70]. Here we wish to study the response of the antiferromagnetic vortex state to these external fields. The kinetic term of the Lagrangian for the Néel vector field reads $\int d^2\mathbf{r} \rho(\partial_t \mathbf{n} - \mathbf{h} \times \mathbf{n})^2/2$ in the presence of the Zeeman coupling $-\hbar \sum_i \mathbf{h} \cdot \mathbf{S}_i$, where $\mathbf{h} \equiv \gamma_e \mathbf{B}$ with magnetic field \mathbf{B} and gyromagnetic ratio γ_e . We assume the applied field to be perpendicular to

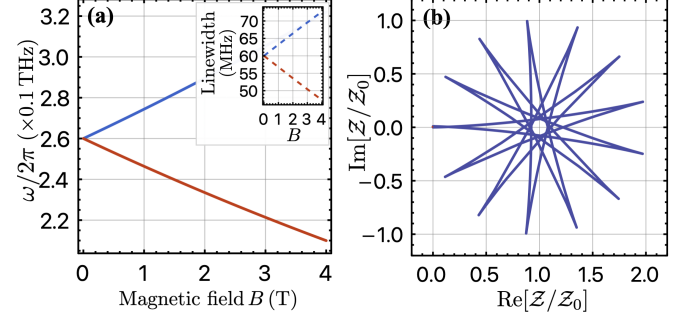


FIG. 2. Vortex dynamics. (a) Dependence of left and right circular vortex oscillation frequencies on the magnetic field. With increasing field, ω_L (red line) decreases while ω_R (blue line) increases. The inset depicts the linewidth of ω_R (blue dashed line) and ω_L (red dashed line) as a function of B field, exhibiting asymmetry at finite magnetic fields. (b) Trajectory of the vortex. Here we set $\gamma = 0$ and $\omega_c = 20$ GHz. The current is assumed to be along the y direction.

the magnetic dot, $\mathbf{h} = h\hat{z}$. Introducing a gauge field $\mathcal{A}_i = \rho\hbar \int d\mathbf{r} \hat{z} \cdot (\mathbf{n} \times \partial_i \mathbf{n})$, the cross term linear in \mathbf{h} takes the form $\mathcal{A}_i \dot{\mathcal{R}}_i$. It generates a Magnus force $\dot{\mathcal{R}} \times \mathcal{B}\hat{z}$ acting on the vortex through the effective field

$$\mathcal{B} = \epsilon_{ij} \partial_{\mathcal{R}_i} \mathcal{A}_j = -\mathcal{M}h\mathcal{N}. \quad (6)$$

When an electric current flows through the metallic antiferromagnetic dot, the s-d coupling between the local magnetic moments and the electron spins polarizes the electrons to follow the orientation of spins on individual sublattices, leading to the adiabatic spin-transfer torque on each sublattice [71, 72]. This effect can be captured by replacing the time derivative with a convective derivative $D_t = \partial_t + \mathbf{u} \cdot \nabla$ in the kinetic term [73], where \mathbf{u} is the drift velocity of the electrons in the current. This leads to a nontrivial term $\rho \int d\mathbf{r} \mathbf{h} \cdot [(\mathbf{u} \cdot \nabla) \mathbf{n} \times \mathbf{n}]$, which gives rise to a Magnus force acting on the vortex transverse to the applied current $-\mathbf{u} \times \mathcal{B}\hat{z}$ [74, 75]. It is analogous to the Magnus force exerted on a vortex line in superconductors when subjected to an electric current [76]. Now, the equation of motion for the vortex in the antiferromagnetic disk is

$$\mathcal{M}\ddot{\mathcal{R}} + 2\mathcal{M}\gamma\dot{\mathcal{R}} + (\mathbf{u} - \dot{\mathcal{R}}) \times \mathcal{B}\hat{z} + \nabla_{\mathcal{R}}\delta\mathcal{U} = 0, \quad (7)$$

where the second term accounts for the friction captured by the Rayleigh dissipation function $(\hbar\alpha s/2) \int d^2\mathbf{r} \dot{\mathbf{n}}^2$ with the Gilbert damping α and spin density s . The friction coefficient $\gamma \equiv \pi\hbar\alpha s/\mathcal{M}$ translates into the linewidth of the vortex oscillation modes, which is about $\gamma \approx 2\pi \times 60$ MHz when $\alpha \sim 10^{-4}$ and $s \sim 1/a^2$. The vortex oscillator is therefore characterized by a high quality factor $\Omega_0/\gamma \gtrsim 4 \times 10^3$ and well-suited for stable and coherent THz signal generation.

The response function of the system $\hat{\chi}(\omega)$ is defined through $\mathcal{R}^T(\omega) = \hat{\chi}(\omega)\mathbf{f}^T(\omega)/\mathcal{M}$, where \mathbf{f} is an external

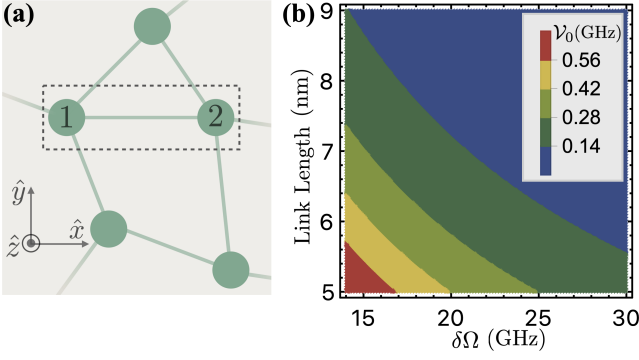


FIG. 3. (a) A patch of an interconnected vortex network. Disks, represented by green dots, are connected by antiferromagnetic links. (b) The coupling strength between vortices as a function of the link length and the frequency difference $\delta\Omega \equiv \Delta - \Omega_0$. In the plot, we set the antiferromagnetic coupling in the link and the easy-axis anisotropy to be $J_A/\hbar \approx 2\pi \times 210$ GHz and $K_A/\hbar \approx 2\pi \times 40$ GHz, respectively. We also set the coupling between the magnetic disk and the link to be $J_A/\hbar \approx 2\pi \times 20$ GHz.

force. From the equation of motion, it is given by

$$\hat{\chi}^{-1}(\omega) = \chi_0^{-1}(\omega) + 2\omega_c\omega\hat{\sigma}_y, \quad (8)$$

where $\omega_c \equiv -\mathcal{B}/(2\mathcal{M}) = \hbar\mathcal{N}/2$ is the effective cyclotron frequency and $\chi_0(\omega) \equiv -(\omega^2 + 2i\gamma\omega - \Omega_0^2)^{-1}$ is the bare response function in the absence of an applied magnetic field. The Pauli matrix $\hat{\sigma}_y$ originates from the breaking of time-reversal symmetry. The poles of $\hat{\chi}$ yields the characteristic frequencies associated with the right and left circular vortex-oscillation modes, $\omega_{R/L} \approx \Omega \pm \omega_c$ with $\Omega = \sqrt{\Omega_0^2 + \omega_c^2}$ and linewidth $\gamma(1 \pm \omega_c/\Omega)$. Note that the applied magnetic field lifts the degeneracy of the two circular modes, while also producing linewidth asymmetry. As depicted in Fig. 2(a), the frequency of the left (right) circular mode is pushed downward (upward) and attains a narrower (broader) linewidth when the field is oriented along the positive \hat{z} -axis. We point out that, importantly, these modes can be excited by an applied in-plane dc current. Consider the scenario where a vortex, initially stationary at the center of the disk, is subjected to a current characterized by an electron drift velocity \mathbf{u} . In this case, the current-induced vortex motion is $\mathcal{Z}(t) = \mathcal{Z}_0[1 - (\omega_R e^{-i\omega_L t} + \omega_L e^{i\omega_R t})/2\Omega]$, where $\mathcal{Z} \equiv \mathcal{R}_x + i\mathcal{R}_y$ represents the vortex position. The finite linewidth ultimately brings the vortex to its stationary position $\mathcal{Z}_0 = 2\omega_c(u_y - iu_x)/\Omega_0^2$, where the restoring force is balanced with the Magnus force exerted by the current. As an example, we depict the vortex trajectory in real space with vanishing damping in Fig. 2(b) for an applied current in y direction. The final stationary position is on the x axis with finite linewidth [77].

Tunable vortex interactions.—A magnetic vortex network requires a coherent interaction between different vortex disks. Here we illustrate that such a coupling can

be mediated via an antiferromagnetic link with gapped magnonic excitations, as sketched in Fig. 3(a). To this end, we consider a microscopic Hamiltonian $H_{\text{link}} = J_A \sum_{\langle i,j \rangle} \mathbf{S}_i \cdot \mathbf{S}_j - K_A \sum_i (\mathbf{S}_i \cdot \hat{x})^2$ describing the quasi-one-dimensional antiferromagnetic coupler. The coefficients J_A and K_A are both positive, standing for the antiferromagnetic coupling and the easy-axis anisotropy along the link (defined as \hat{x} -axis), respectively. The interaction between vortices is primarily mediated by magnon excitations with small momentum k , and the corresponding spectrum is $\omega_k = Ak^2 + \Delta$ [77]. Here, $A \equiv J_A Sa^2/(\hbar E_g)$ is the exchange stiffness and $\Delta \equiv 2SE_g J_A/\hbar$ is the excitation gap, where $E_g = \sqrt{(1 + K_A/J_A)^2 - 1}$. We consider two magnetic dots coupled to the left and right ends of the link through exchange coupling:

$$H'/\mathcal{J}_A = \mathbf{n}_1(R\hat{x}) \cdot \mathbf{n}_{\text{link}}(0) + \mathbf{n}_2(-R\hat{x}) \cdot \mathbf{n}_{\text{link}}(L), \quad (9)$$

where \mathcal{J}_A is the coupling strength and $\mathbf{n}_1(R\hat{x})$, $\mathbf{n}_2(-R\hat{x})$ denote the Néel vectors at the right side of the first disk and the left side of the second disk, respectively; $\mathbf{n}_{\text{link}}(0)$, $\mathbf{n}_{\text{link}}(L)$ stand for the Néel vector field of the link (with total length L) evaluated at two ends. We again adopt the collective coordinates for vortices, which yields $n_x(\pm R\hat{x}) \approx \pm 1 - \mathcal{X}$, $n_y(\pm R\hat{x}) \approx -\mathcal{N}$, $n_z(\pm R\hat{x}) \approx \pm p\mathcal{X}$ [77] with dimensionless displacement (\mathcal{X}, \mathcal{Y}) in units of the magnetic exchange length λ_0 to linear order in \mathcal{X} and \mathcal{Y} . Here, $p, \mathcal{N} = \pm 1$ are the polarity and the charge of the vortex, respectively.

We focus on the scenario where the vortex oscillation frequency falls below the band gap Δ , ensuring that the vortex dynamics do not excite magnons in the link. Otherwise, the link could result in extra damping and dissipative coupling within the vortices [2, 79–81]. To derive the coherent vortex-vortex interaction mediated by the virtual magnons, we trace out the the degrees of freedom of the link by applying the Schrieffer-Wolff transformation [1], which yields

$$\mathcal{V} \approx \mathcal{V}_0 [-p_1 p_2 \mathcal{X}_1 \mathcal{X}_2 + \mathcal{N}_1 \mathcal{N}_2 \mathcal{Y}_1 \mathcal{Y}_2]. \quad (10)$$

Note that, importantly, both polarity and topological number can change the sign of the interaction. We have focused on the case without external magnetic field for simplicity. The detailed derivation and general discussion are provided in SM [77]. The coupling strength $\mathcal{V}_0 = \mathcal{J}_A^2 \chi_{\perp}(\Omega_0, L)/(2\hbar)$ is determined by the transversal susceptibility of the antiferromagnetic link evaluated to be

$$\chi_{\perp}(\Omega_0, L) \approx \frac{\alpha_0 e^{-k_F L}}{A(k_F/a)}, \quad \text{with } k_F = \sqrt{\frac{\Delta - \Omega_0}{A}}, \quad (11)$$

where α_0 is a dimensionless factor of order one and $1/k_F$ defines a characteristic length that increases as the vortex oscillation frequency approaches the magnon band edge. As we show in Fig. 3(b), the coupling \mathcal{V}_0 decays as $\exp(-k_F L)$ when the link length increases. On

the other hand, for given L , the coupling scales nonlinearly with the vortex oscillation frequency: $\mathcal{V}_0 \propto \exp\left[-(L/\sqrt{A})\sqrt{\delta\Omega}\right]/\sqrt{\delta\Omega}$ with $\delta\Omega = \Delta - \Omega_0$. This offers a convenient way to tune the coupling between vortices by adjusting the vortex resonance frequency, for instance, via a magnetic field. We finally point out that, while reducing $\delta\Omega$ can enhance the coupling, we still require $\delta\Omega$ to be comparable or larger than \mathcal{J}_A to validate the perturbation theory employed in our discussion [1].

Summary and outlook.—We explored the feasibility of sustaining a stable vortex state in an antiferromagnetic nanodot encircled by a heavy metal. We reveal that in the presence of iDMI, a vortex state can be stabilized, akin to the formation of a vortex by rotation in a superfluid. The vortex state serves as a stable generator of coherent THz signals, which can be further modulated with magnetic fields and effectively excited by electric currents, heralding a range of innovative applications. Furthermore, by linking two nanodots through an antiferromagnetic coupler, virtual magnons enable tunable interactions between vortices in the dots.

Building upon our study, one could envision a range of interesting future research directions. Firstly, in addition to investigating the realization of non-volatile logic operations and unconventional computation within a vortex network, one could utilize nanodisks as meta-atoms to construct metamaterials, offering a fertile ground for exploring various phenomena [83–87]. Secondly, while our focus has been on the coherent coupling between vortices, future studies can explore the dissipative coupling between vortices, which naturally occurs when the vortex resonance frequency falls within the magnon band of the coupler. This leads to a dissipatively interconnected vortex network, providing an ideal platform for examining the utilization of dissipation or for investigating various non-Hermitian magnonic phases, which have recently garnered considerable interest in the community [88–93]. Lastly, the nanoscale size of the vortex state not only facilitates high-density integration on microchips but also opens up possibilities for harnessing its quantum properties [94]. For example, there is potential for using the vortex state as a qubit or integrating it into existing quantum computation platforms.

Acknowledgments. This work was supported by the Georg H. Endress Foundation and by the Swiss National Science Foundation, NCCR SPIN (grant number 51NF40-180604). S.K.K. was supported by the Brain Pool Plus Program through the National Research Foundation of Korea funded by the Ministry of Science and ICT (2020H1D3A2A03099291).

[1] S. S. Parkin, M. Hayashi, and L. Thomas, Magnetic domain-wall racetrack memory, *Science* **320**, 190 (2008).

- [2] J. Zang, V. Cros, and A. Hoffmann, eds., *Topology in Magnetism* (Springer International Publishing, 2018).
- [3] Y. Tserkovnyak and J. Xiao, Energy storage via topological spin textures, *Phys. Rev. Lett.* **121**, 127701 (2018).
- [4] Y. Liu, R. K. Lake, and J. Zang, Binding a hopfion in a chiral magnet nanodisk, *Phys. Rev. B* **98**, 174437 (2018).
- [5] J. Tang, Y. Wu, W. Wang, L. Kong, B. Lv, W. Wei, J. Zang, M. Tian, and H. Du, Magnetic skyrmion bundles and their current-driven dynamics, *Nat. Nanotechnol.* **16**, 1086 (2021).
- [6] R. Zarzuela, V. K. Bharadwaj, K.-W. Kim, J. Sinova, and K. Everschor-Sitte, Stability and dynamics of in-plane skyrmions in collinear ferromagnets, *Phys. Rev. B* **101**, 054405 (2020).
- [7] R. Cheng, M. Li, A. Sapkota, A. Rai, A. Pokhrel, T. Mewes, C. Mewes, D. Xiao, M. De Graef, and V. Sokalski, Magnetic domain wall skyrmions, *Phys. Rev. B* **99**, 184412 (2019).
- [8] C. Psaroudaki, E. Peraticos, and C. Panagopoulos, Skyrmion qubits: Challenges for future quantum computing applications, *Appl. Phys. Lett.* **123** (2023).
- [9] C. Psaroudaki and C. Panagopoulos, Skyrmion qubits: A new class of quantum logic elements based on nanoscale magnetization, *Phys. Rev. Lett.* **127**, 067201 (2021).
- [10] J. Lan, W. Yu, R. Wu, J. Xiao, *et al.*, Spin-wave diode, *Phys. Rev. X* **5**, 041049 (2015).
- [11] J. Zou, S. Bosco, B. Pal, S. S. P. Parkin, J. Klinovaja, and D. Loss, Quantum computing on magnetic racetracks with flying domain wall qubits, *Phys. Rev. Res.* **5**, 033166 (2023).
- [12] Z. Jin, X. Yao, Z. Wang, H. Yuan, Z. Zeng, W. Wang, Y. Cao, and P. Yan, Nonlinear topological magnon spin hall effect, *Phys. Rev. Lett.* **131**, 166704 (2023).
- [13] J. Xia, X. Zhang, X. Liu, Y. Zhou, and M. Ezawa, Universal quantum computation based on nanoscale skyrmion helicity qubits in frustrated magnets, *Phys. Rev. Lett.* **130**, 106701 (2023).
- [14] M. W. Daniels, W. Yu, R. Cheng, J. Xiao, D. Xiao, *et al.*, Topological spin hall effects and tunable skyrmion hall effects in uniaxial antiferromagnetic insulators, *Phys. Rev. B* **99**, 224433 (2019).
- [15] S. Takei and M. Mohseni, Quantum control of topological defects in magnetic systems, *Phys. Rev. B* **97**, 064401 (2018).
- [16] S. Takei, Y. Tserkovnyak, and M. Mohseni, Spin superfluid josephson quantum devices, *Phys. Rev. B* **95**, 144402 (2017).
- [17] X. Wang, H. Yuan, and X. Wang, A theory on skyrmion size, *Communications Physics* **1**, 31 (2018).
- [18] J. Zou, S. Zhang, and Y. Tserkovnyak, Topological transport of deconfined hedgehogs in magnets, *Phys. Rev. Lett.* **125**, 267201 (2020).
- [19] X. S. Wang, A. Qaiumzadeh, and A. Brataas, Current-driven dynamics of magnetic hopfions, *Phys. Rev. Lett.* **123**, 147203 (2019).
- [20] Y. Liu, W. Hou, X. Han, and J. Zang, Three-dimensional dynamics of a magnetic hopfion driven by spin transfer torque, *Phys. Rev. Lett.* **124**, 127204 (2020).
- [21] Y. Tserkovnyak, J. Zou, S. K. Kim, and S. Takei, Quantum hydrodynamics of spin winding, *Phys. Rev. B* **102**, 224433 (2020).
- [22] J. Zou, S. K. Kim, and Y. Tserkovnyak, Topological transport of vorticity in heisenberg magnets, *Phys. Rev. B* **99**, 180402 (2019).

- [23] R. Zarzuela and J. Sinova, Spin-transfer and topological hall effects in itinerant frustrated magnets, *Phys. Rev. B* **108**, 134402 (2023).
- [24] Y. Yamane, O. Gomonay, and J. Sinova, Dynamics of noncollinear antiferromagnetic textures driven by spin current injection, *Phys. Rev. B* **100**, 054415 (2019).
- [25] C. Dao, J. Zou, E. Kleinherbers, and Y. Tserkovnyak, Topological transport of vorticity on curved magnetic membranes, *arXiv:2311.00323* (2023).
- [26] T. Shinjo, T. Okuno, R. Hassdorf, K. Shigeto, and T. Ono, Magnetic vortex core observation in circular dots of permalloy, *Science* **289**, 930 (2000).
- [27] A. Wachowiak, J. Wiebe, M. Bode, O. Pietzsch, M. Morgenstern, and R. Wiesendanger, Direct observation of internal spin structure of magnetic vortex cores, *Science* **298**, 577 (2002).
- [28] A. Dussaux, B. Georges, J. Grollier, V. Cros, A. Khvalkovskiy, A. Fukushima, M. Konoto, H. Kubota, K. Yakushiji, S. Yuasa, *et al.*, Large microwave generation from current-driven magnetic vortex oscillators in magnetic tunnel junctions, *Nat. Commun.* **1**, 1 (2010).
- [29] S. Wintz, V. Tiberkevich, M. Weigand, J. Raabe, J. Lindner, A. Erbe, A. Slavin, and J. Fassbender, Magnetic vortex cores as tunable spin-wave emitters, *Nat. Nanotechnol.* **11**, 948 (2016).
- [30] S. Choi, K.-S. Lee, K. Y. Guslienko, and S.-K. Kim, Strong radiation of spin waves by core reversal of a magnetic vortex and their wave behaviors in magnetic nanowire waveguides, *Phys. Rev. Lett.* **98**, 087205 (2007).
- [31] K. Yamada, S. Kasai, Y. Nakatani, K. Kobayashi, H. Kohno, A. Thiaville, and T. Ono, Electrical switching of the vortex core in a magnetic disk, *Nat. Mater.* **6**, 270 (2007).
- [32] K. Y. Guslienko, K.-S. Lee, and S.-K. Kim, Dynamic origin of vortex core switching in soft magnetic nanodots, *Phys. Rev. Lett.* **100**, 027203 (2008).
- [33] B. Pigeau, G. De Loubens, O. Klein, A. Riegler, F. Lochner, G. Schmidt, L. Molenkamp, V. Tiberkevich, and A. Slavin, A frequency-controlled magnetic vortex memory, *Appl. Phys. Lett.* **96** (2010).
- [34] S. Bohlens, B. Krüger, A. Drews, M. Bolte, G. Meier, and D. Pfannkuche, Current controlled random-access memory based on magnetic vortex handedness, *Appl. Phys. Lett.* **93** (2008).
- [35] G. Hrkac, P. S. Keatley, M. T. Bryan, and K. Butler, Magnetic vortex oscillators, *J. Phys. D: Appl. Phys.* **48**, 453001 (2015).
- [36] H. Jung, Y.-S. Choi, K.-S. Lee, D.-S. Han, Y.-S. Yu, M.-Y. Im, P. Fischer, and S.-K. Kim, Logic operations based on magnetic-vortex-state networks, *Acs Nano* **6**, 3712 (2012).
- [37] S. Shreya, M. Zamani, Y. Rezaeiyan, H. Ghanatian, T. Böhnert, A. S. Jenkins, R. Ferreira, H. Farkhani, and F. Moradi, Memory and communication-in-logic using vortex and precessional oscillations in a magnetic tunnel junction, *IEEE Magn. Lett.* **13**, 1 (2022).
- [38] K. A. Omari and T. J. Hayward, Chirality-based vortex domain-wall logic gates, *Phys. Rev. Appl.* **2**, 044001 (2014).
- [39] J. Torrejon, M. Riou, F. A. Araujo, S. Tsunegi, G. Khalsa, D. Querlioz, P. Bortolotti, V. Cros, K. Yakushiji, A. Fukushima, *et al.*, Neuromorphic computing with nanoscale spintronic oscillators, *Nature* **547**, 428 (2017).
- [40] C. Yun, Y. Wu, Z. Liang, W. Yang, H. Du, S. Liu, J. Han, Y. Hou, J. Yang, and Z. Luo, Magnetic anisotropy-controlled vortex nano-oscillator for neuromorphic computing, *Front. Phys.* **10**, 1019881 (2022).
- [41] S. Shreya, A. Jenkins, Y. Rezaeiyan, R. Li, T. Böhnert, L. Benetti, R. Ferreira, F. Moradi, and H. Farkhani, Granular vortex spin-torque nano oscillator for reservoir computing, *Sci. Rep.* **13**, 16722 (2023).
- [42] B. Van Waeyenberge, A. Puzic, H. Stoll, K. Chou, T. Tylliszczak, R. Hertel, M. Fähnle, H. Brückl, K. Rott, G. Reiss, *et al.*, Magnetic vortex core reversal by excitation with short bursts of an alternating field, *Nature* **444**, 461 (2006).
- [43] M. Curcic, B. Van Waeyenberge, A. Vansteenkiste, M. Weigand, V. Sackmann, H. Stoll, M. Fähnle, T. Tylliszczak, G. Woltersdorf, C. H. Back, and G. Schütz, Polarization selective magnetic vortex dynamics and core reversal in rotating magnetic fields, *Phys. Rev. Lett.* **101**, 197204 (2008).
- [44] Y. Liu, S. Gliga, R. Hertel, and C. Schneider, Current-induced magnetic vortex core switching in a permalloy nanodisk, *Appl. Phys. Lett.* **91** (2007).
- [45] X. Fu, S. D. Pollard, B. Chen, B.-K. Yoo, H. Yang, and Y. Zhu, Optical manipulation of magnetic vortices visualized in situ by lorentz electron microscopy, *Sci. Adv.* **4**, eaat3077 (2018).
- [46] K. Yamada, S. Kasai, Y. Nakatani, K. Kobayashi, and T. Ono, Current-induced switching of magnetic vortex core in ferromagnetic elliptical disks, *Appl. Phys. Lett.* **96** (2010).
- [47] V. P. Kravchuk, Y. Gaididei, and D. D. Sheka, Nucleation of a vortex-antivortex pair in the presence of an immobile magnetic vortex, *Phys. Rev. B* **80**, 100405 (2009).
- [48] M. Kammerer, M. Weigand, M. Curcic, M. Noske, M. Sproll, A. Vansteenkiste, B. Van Waeyenberge, H. Stoll, G. Woltersdorf, C. H. Back, *et al.*, Magnetic vortex core reversal by excitation of spin waves, *Nat. Commun.* **2**, 279 (2011).
- [49] R. Hertel, S. Gliga, M. Fähnle, and C. M. Schneider, Ultrafast nanomagnetic toggle switching of vortex cores, *Phys. Rev. Lett.* **98**, 117201 (2007).
- [50] S. K. Kim and Y. Tserkovnyak, Fast vortex oscillations in a ferrimagnetic disk near the angular momentum compensation point, *Appl. Phys. Lett.* **111** (2017).
- [51] J. Shibata, Y. Nakatani, G. Tatara, H. Kohno, and Y. Otani, Current-induced magnetic vortex motion by spin-transfer torque, *Phys. Rev. B* **73**, 020403 (2006).
- [52] Z. Gao, F. Wang, X. Zhao, T. Wang, J. Hu, and P. Yan, Interplay between spin wave and magnetic vortex, *Physical Review B* **107**, 214418 (2023).
- [53] Z.-X. Li, Z. Wang, Z. Zhang, Y. Cao, and P. Yan, Third-order topological insulator in three-dimensional lattice of magnetic vortices, *Phys. Rev. B* **103**, 214442 (2021).
- [54] V. Pribiag, I. Krivorotov, G. Fuchs, P. Braganca, O. Ozatay, J. Sankey, D. Ralph, and R. Buhrman, Magnetic vortex oscillator driven by dc spin-polarized current, *Nat. Phys.* **3**, 498 (2007).
- [55] Y.-S. Yu, D.-S. Han, M.-W. Yoo, K.-S. Lee, Y.-S. Choi, H. Jung, J. Lee, M.-Y. Im, P. Fischer, and S.-K. Kim, Resonant amplification of vortex-core oscillations by coherent magnetic-field pulses, *Sci. Rep.* **3**, 1301 (2013).
- [56] A. Vogel, A. Drews, T. Kamionka, M. Bolte, and G. Meier, Influence of dipolar interaction on vortex dynamics in arrays of ferromagnetic disks, *Phys. Rev. Lett.*

- 105**, 037201 (2010).
- [57] S. Sugimoto, Y. Fukuma, S. Kasai, T. Kimura, A. Barman, and Y. Otani, Dynamics of coupled vortices in a pair of ferromagnetic disks, *Phys. Rev. Lett.* **106**, 197203 (2011).
 - [58] M. Kuepferling, A. Casiraghi, G. Soares, G. Durin, F. Garcia-Sanchez, L. Chen, C. H. Back, C. H. Marrows, S. Tacchi, and G. Carlotti, Measuring interfacial dzyaloshinskii-moriya interaction in ultrathin magnetic films, *Rev. Mod. Phys.* **95**, 015003 (2023).
 - [59] Y. Tserkovnyak and J. Zou, Quantum hydrodynamics of vorticity, *Phys. Rev. Research* **1**, 033071 (2019).
 - [60] M. R. K. Akanda, I. J. Park, and R. K. Lake, Interfacial dzyaloshinskii-moriya interaction of antiferromagnetic materials, *Phys. Rev. B* **102**, 224414 (2020).
 - [61] A. Qaiumzadeh, I. A. Ado, R. A. Duine, M. Titov, and A. Brataas, Theory of the interfacial dzyaloshinskii-moriya interaction in rashba antiferromagnets, *Phys. Rev. Lett.* **120**, 197202 (2018).
 - [62] O. M. Volkov, D. D. Sheka, Y. Gaididei, V. P. Kravchuk, U. K. Röbber, J. Fassbender, and D. Makarov, Mesoscale dzyaloshinskii-moriya interaction: geometrical tailoring of the magnetochirality, *Sci. Rep.* **8**, 866 (2018).
 - [63] C. J. Pethick and H. Smith, *Bose-Einstein condensation in dilute gases* (Cambridge university press, 2008).
 - [64] One can also consider a disk with a larger radius. In this case, the equilibrium position of the vortex may not be at the center of the disk.
 - [65] K. Y. Guslienko, V. Novosad, Y. Otani, H. Shima, and K. Fukamichi, Field evolution of magnetic vortex state in ferromagnetic disks, *Appl. Phys. Lett.* **78**, 3848 (2001).
 - [66] Here, we have omitted the constant term independent of the vortex number. Specifically, for $\mathcal{N} = 1$, the potential energy evaluates to be $\mathcal{U} = \pi(7/2 - 2\ln 2)\mathcal{J} - 2\pi D$.
 - [67] E. G. Tveten, A. Qaiumzadeh, and A. Brataas, Antiferromagnetic domain wall motion induced by spin waves, *Phys. Rev. Lett.* **112**, 147204 (2014).
 - [68] F. L. A. Machado, P. R. T. Ribeiro, J. Holanda, R. L. Rodríguez-Suárez, A. Azevedo, and S. M. Rezende, Spin-flop transition in the easy-plane antiferromagnet nickel oxide, *Phys. Rev. B* **95**, 104418 (2017).
 - [69] S. D. Bader and S. Parkin, Spintronics, *Annu. Rev. Condens. Matter Phys.* **1**, 71 (2010).
 - [70] V. Baltz, A. Manchon, M. Tsoi, T. Moriyama, T. Ono, and Y. Tserkovnyak, Antiferromagnetic spintronics, *Rev. Mod. Phys.* **90**, 015005 (2018).
 - [71] R. Cheng, J. Xiao, Q. Niu, and A. Brataas, Spin pumping and spin-transfer torques in antiferromagnets, *Phys. Rev. Lett.* **113**, 057601 (2014).
 - [72] K. M. D. Hals, Y. Tserkovnyak, and A. Brataas, Phenomenology of current-induced dynamics in antiferromagnets, *Phys. Rev. Lett.* **106**, 107206 (2011).
 - [73] A. C. Swaving and R. A. Duine, Current-induced torques in continuous antiferromagnetic textures, *Phys. Rev. B* **83**, 054428 (2011).
 - [74] S. Dasgupta and J. Zou, Zeeman term for the néel vector in a two sublattice antiferromagnet, *Phys. Rev. B* **104**, 064415 (2021).
 - [75] S. Dasgupta, S. K. Kim, and O. Tchernyshyov, Gauge fields and related forces in antiferromagnetic soliton physics, *Phys. Rev. B* **95**, 220407 (2017).
 - [76] P. G. DE GENNES and J. MATRICON, Collective modes of vortex lines in superconductors of the second kind, *Rev. Mod. Phys.* **36**, 45 (1964).
 - [77] See Supplemental Material for (i) Derivation of vortex-vortex interaction and (ii) Trajectories of the vortex.
 - [2] L. Trifunovic, F. L. Pedrocchi, and D. Loss, Long-distance entanglement of spin qubits via ferromagnet, *Phys. Rev. X* **3**, 041023 (2013).
 - [79] B. Hetényi, A. Mook, J. Klinovaja, and D. Loss, Long-distance coupling of spin qubits via topological magnons, *Phys. Rev. B* **106**, 235409 (2022).
 - [80] J. Zou, S. Bosco, E. Thingstad, J. Klinovaja, and D. Loss, Dissipative spin-wave diode and nonreciprocal magnonic amplifier, *Phys. Rev. Lett.* **132**, 036701 (2024).
 - [81] J. Zou, S. Bosco, and D. Loss, Spatially correlated classical and quantum noise in driven qubits: The good, the bad, and the ugly, *arXiv:2308.03054* (2023).
 - [1] S. Bravyi, D. P. DiVincenzo, and D. Loss, Schrieffer-wolff transformation for quantum many-body systems, *Ann. Phys.* **326**, 2793 (2011).
 - [83] Z.-X. Li, Y. Cao, and P. Yan, Topological insulators and semimetals in classical magnetic systems, *Phys. Rep.* **915**, 1 (2021).
 - [84] S. K. Kim and Y. Tserkovnyak, Chiral edge mode in the coupled dynamics of magnetic solitons in a honeycomb lattice, *Phys. Rev. Lett.* **119**, 077204 (2017).
 - [85] Z. Li, Y. Cao, P. Yan, and X. Wang, Higher-order topological solitonic insulators, *npj Computational Materials* **5**, 107 (2019).
 - [86] Z.-X. Li, C. Wang, Y. Cao, and P. Yan, Edge states in a two-dimensional honeycomb lattice of massive magnetic skyrmions, *Phys. Rev. B* **98**, 180407 (2018).
 - [87] Z.-X. Li, Z. Wang, Y. Cao, H. W. Zhang, and P. Yan, Robust edge states in magnetic soliton racetrack, *Phys. Rev. B* **103**, 054438 (2021).
 - [88] T. Yu, J. Zou, B. Zeng, J. Rao, and K. Xia, Non-hermitian topological magnonics, *arXiv:2306.04348* (2023).
 - [89] H. M. Hurst and B. Flebus, Non-hermitian physics in magnetic systems, *J. Appl. Phys.* **132**, 220902 (2022).
 - [90] W. Yu, J. Wang, H. Yuan, J. Xiao, *et al.*, Prediction of attractive level crossing via a dissipative mode, *Phys. Rev. Lett.* **123**, 227201 (2019).
 - [91] J. Zou, S. Zhang, and Y. Tserkovnyak, Bell-state generation for spin qubits via dissipative coupling, *Phys. Rev. B* **106**, L180406 (2022).
 - [92] Y. Ashida, Z. Gong, and M. Ueda, Non-hermitian physics, *Adv. Phys.* **69**, 249 (2020).
 - [93] K. Nakata, J. Zou, J. Klinovaja, and D. Loss, Magnonic φ josephson junctions and synchronized precession, *arXiv:2403.01625* (2024).
 - [94] H. Yuan, Y. Cao, A. Kamra, R. A. Duine, and P. Yan, Quantum magnonics: When magnon spintronics meets quantum information science, *Phys. Rep.* **965**, 1 (2022).

Supplemental Material for “Tunable Ultrafast Dynamics of Antiferromagnetic Vortices in Nanoscale Dots”

(i) Derivation of vortex-vortex interaction

Here we provide detailed derivations and discussions on the coherent interactions between vortices connected via an antiferromagnetic coupler. Let us first focus on the Hamiltonian describing the exchange coupling between the vortex disk and the link:

$$H'/\mathcal{J}_A = \mathbf{n}_1(R\hat{x}) \cdot \mathbf{n}_{\text{link}}(0) + \mathbf{n}_2(-R\hat{x}) \cdot \mathbf{n}_{\text{link}}(L), \quad (\text{S1})$$

where \mathcal{J}_A is the coupling strength. Here $\mathbf{n}_1(R\hat{x})$ and $\mathbf{n}_2(-R\hat{x})$ stands for the Néel vector fields of the left and right magnetic disks evaluated at $\mathbf{r} = R\hat{x}$ and $\mathbf{r} = -R\hat{x}$ (with the origins at the center of the disks). We adopt the collective coordinates $\mathbf{n}(\mathbf{r}, t) = \mathbf{n}_0(\mathbf{r} - \mathcal{R}(t))$, with $\mathbf{n}_0(\mathbf{r})$ being the ansatz that we assume in the main text. It can be written as:

$$n_x(\mathbf{r}) = \frac{2x/\lambda_0}{(x/\lambda_0)^2 + (y/\lambda_0)^2 + 1}, \quad n_y(\mathbf{r}) = \frac{2y/\lambda_0}{(x/\lambda_0)^2 + (y/\lambda_0)^2 + 1}, \quad n_z(\mathbf{r}) = \frac{2}{(x/\lambda_0)^2 + (y/\lambda_0)^2 + 1} - 1, \quad (\text{S2})$$

in the Cartesian coordinate with λ_0 being the characteristic length. We recall that we consider a disk with a radius comparable to this length $R \sim \lambda_0$. Then we have:

$$\begin{aligned} n_x(R\hat{x}) &= \frac{2(1 - \mathcal{X})}{(1 - \mathcal{X})^2 + \mathcal{Y}^2 + 1} \approx 1 - \mathcal{X}, \\ n_y(R\hat{x}) &= \frac{2(-\mathcal{Y})}{(1 - \mathcal{X})^2 + \mathcal{Y}^2 + 1} \approx -\mathcal{Y}, \\ n_z(R\hat{x}) &= \frac{2}{(1 - \mathcal{X})^2 + \mathcal{Y}^2 + 1} - 1 \approx +\mathcal{X}, \end{aligned} \quad (\text{S3})$$

where we have introduced the dimensionless coordinate $\mathcal{R}/\lambda_0 \equiv (\mathcal{X}, \mathcal{Y})$ in units of λ_0 . Similarly one can find that

$$n_x(-R\hat{x}) \approx -1 - \mathcal{X}, \quad n_y(-R\hat{x}) \approx -\mathcal{Y}, \quad n_z(-R\hat{x}) \approx -\mathcal{X}. \quad (\text{S4})$$

We remark that we have used the ansatz with positive polarity $p = +1$ and positive vortex number $\mathcal{N} = +1$. When the polarity flips, we have $n_z \rightarrow -n_z$, and when $\mathcal{N} = -1$, it results in $n_y \rightarrow -n_y$. Thus, the Hamiltonian (S1) can be written as

$$\begin{aligned} H'/\mathcal{J}_A &= (1 - \mathcal{X}_1)n_x(0) + (-1 - \mathcal{X}_2)n_x(L) - \mathcal{Y}_1n_y(0) - \mathcal{Y}_2n_y(L) + \mathcal{X}_1n_z(0) - \mathcal{X}_2n_z(L), \\ &= (1 - \mathcal{X}_1)n_x(0) + (-1 - \mathcal{X}_2)n_x(L) + \frac{\mathcal{X}_1 - i\mathcal{Y}_1}{2i}n^+(0) - \frac{\mathcal{X}_1 + i\mathcal{Y}_1}{2i}n^-(0) \\ &\quad + \frac{\mathcal{X}_2 - i\mathcal{Y}_2}{2i}n^-(L) - \frac{\mathcal{X}_2 + i\mathcal{Y}_2}{2i}n^+(L) \end{aligned} \quad (\text{S5})$$

where we have dropped the sub-index ‘link’ for notational convenience and introduced $n^+ \equiv n_y + in_z$, $n^- \equiv n_y - in_z$. To proceed, we quantize the vortex motion in the terms of the operators for left and right circular modes d_L , d_L^\dagger and d_R , d_R^\dagger . Then we have

$$\mathcal{X} + i\mathcal{Y} = \sqrt{2}\lambda(d_R + d_L^\dagger), \quad (\text{S6})$$

where $\lambda = \sqrt{\hbar/(2\mathcal{M}\Omega)}/\lambda_0$ is the dimensionless harmonic length of the confining potential of the vortex (with $\Omega = \sqrt{\Omega_0^2 + \omega_c^2}$).

We now focus on the microscopic Hamiltonian $H_{\text{link}} = J_A \sum_{\langle i,j \rangle} \mathbf{S}_i \cdot \mathbf{S}_j - K_A \sum_i (\mathbf{S}_i \cdot \hat{x})^2$ of the quasi-one-dimensional (two-sublattice) antiferromagnetic coupler. Here, J_A and K_A are both positive, standing for the antiferromagnetic coupling and the easy \hat{x} anisotropy along the link, respectively. We introduce the Holstein-Primakoff transformation

and keep up to the lowest order: $S_A^+ \approx \sqrt{2S}a$ and $S_A^x = S - a^\dagger a$ for site A and $S_B^+ \approx \sqrt{2S}b^\dagger$ and $S_A^x = -S + a^\dagger a$ for site B with $S^\pm \equiv S_y \pm iS_z$. Then this Hamiltonian can be written as

$$H_{\text{link}} = 2SJ_A \sum_k \left[(K_A/J_A + 1)(a_k^\dagger a_k + b_k^\dagger b_k) + \gamma_k(a_k b_k + a_k^\dagger b_k^\dagger) \right], \quad (\text{S7})$$

in the momentum space with $\gamma_k = (e^{ik} + e^{-ik})/2 = \cos k$ (we use dimensionless k by setting the spacing $a = 1$ for simplicity). It can be diagonalized by applying the Bogoliubov transformation

$$a_k = u_k \alpha_k + v_k \beta_k^\dagger, \quad b_k = u_k \beta_k + v_k \alpha_k^\dagger, \quad (\text{S8})$$

Here, $u_k = \cosh \eta_k$ and $v_k = \sinh \eta_k$ with η_k determined by $\tanh 2\eta_k = -\gamma_k/(1 + K_A/J_A)$. Then the Hamiltonian is diagonal in terms of operator α_k and β_k with the dispersion being

$$\hbar\omega_k = 2SJ_A \sqrt{E_g^2 + k^2}, \quad \text{with } E_g = \sqrt{(1 + K_A/J_A)^2 - 1}. \quad (\text{S9})$$

For magnonic excitations with small k , the spectrum is given by

$$\omega_k \approx Ak^2 + \Delta, \quad \text{with } \Delta = \frac{2SJ_A E_g}{\hbar}, \quad A = \frac{SJ_A}{\hbar E_g}. \quad (\text{S10})$$

The second-order effective interaction between the vortices can be obtained by employing a perturbative Schrieffer-Wolff transformation [1]:

$$\mathcal{V} = -\frac{i}{2\hbar} \lim_{\eta \rightarrow 0^+} \int_0^\infty dt e^{-\eta t} [H'(t), H'], \quad (\text{S11})$$

where $H'(t)$ is in the interaction picture. We then have the following effective interaction between vortices:

$$\mathcal{V} = -\frac{\lambda^2 \mathcal{J}_A^2}{4\hbar} \left\{ \left[\chi_\perp(-\omega_R) d_{1R}^\dagger + \chi_\perp(\omega_L) d_{1L} \right] (d_{2R}^\dagger + d_{2L}) + \left[\chi_\perp(-\omega_L) d_{2L}^\dagger + \chi(\omega_R) d_{2R} \right] (d_{1L}^\dagger + d_{1R}) \right\} + \text{h.c.}, \quad (\text{S12})$$

where the transversal susceptibility $\chi_\perp(\omega) \equiv \chi_\perp(\omega, L)$ (we have dropped L for simplicity) is defined as

$$\begin{aligned} \chi_\perp(\omega) &= -i \int_0^\infty dt e^{-i\omega t} [n^+(t, L), n^-(0, 0)] \\ &= -\frac{i}{2S} \int_0^\infty dt e^{-i\omega t} [a_L(t) - b_L^\dagger(t), a_0^\dagger - b_0]. \end{aligned} \quad (\text{S13})$$

Here a_L, b_L, a_0, b_0 are magnon operators on site L and site 0 (L is the length of the coupler). We have used Néel vector $\mathbf{n} \equiv (\mathbf{S}_A - \mathbf{S}_B)/2S$, and we have neglected the longitudinal susceptibility in the interaction (S12) since it is suppressed by temperature [2]. To evaluate Eq. (S13), we write the expression in terms of α_k, β_k in momentum space which eventually yields:

$$\begin{aligned} \chi_\perp(\omega) &= -\frac{i}{2S} \int_0^\infty dt e^{-i\omega t - \eta t} \int \frac{dk}{2\pi} e^{ikL} (u_k - v_k)^2 (e^{-i\omega_k t} - e^{i\omega_k t}) \\ &= \frac{1}{2S} \int \frac{dk}{2\pi} e^{ikL} (u_k - v_k)^2 \left(\frac{1}{\omega - \omega_k - i\eta} - \frac{1}{\omega + \omega_k - i\eta} \right), \end{aligned} \quad (\text{S14})$$

where

$$(u_k - v_k)^2 = \cosh 2\eta_k - \sinh 2\eta_k = \frac{1 - \tanh(2\eta_k)}{\sqrt{1 - \tanh^2(2\eta_k)}} = \frac{2SJ_A(1 + K_A/J_A + \gamma_k)}{\hbar\omega_k}. \quad (\text{S15})$$

We note that Eq. (S14) can be converted into a complex integral. When $\omega > 0$, the main contribution of the integral comes from the pole $k = ik_F$ with $k_F^2 = (\Delta - \omega)/A$, which leads to:

$$\chi_\perp(\omega > 0) \approx -\frac{(u_{ik_F} - v_{ik_F})^2}{4SAk_F} e^{-k_F L} = -\frac{\alpha_0}{Ak_F} e^{-k_F L}. \quad (\text{S16})$$

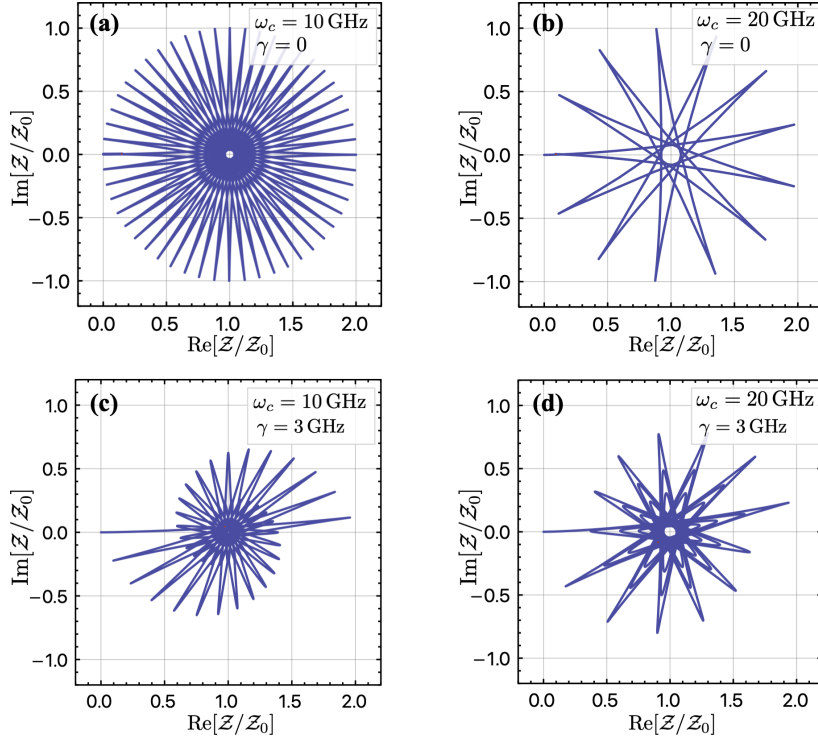


FIG. S4. Vortex trajectory. We plot the trajectories of the vortex with a current in the y direction for (a) $\omega_c = 10$ GHz and zero damping, (b) $\omega_c = 20$ GHz and zero damping, (c) $\omega_c = 10$ GHz and $\gamma = 3$ GHz, and (d) $\omega_c = 20$ GHz and $\gamma = 3$ GHz.

Similarly, for $\omega < 0$, the main contribution still comes from $k = ik_F$ with $k_F^2 = (\Delta - |\omega|)/A$. Thus we have $\chi_\perp(\omega < 0) = \chi_\perp(|\omega| > 0)$. Here α_0 is a dimensionless numeric factor:

$$\alpha_0 = \frac{1}{4S}(u_{ik_F} - v_{ik_F})^2 = \frac{1}{4S}\sqrt{\frac{K_A/J_A + 2 + k_F^2/2}{K_A/J_A - k_F^2/2}} \approx \frac{1}{4S}\sqrt{1 + \frac{2J_A}{K_A}}, \quad (\text{S17})$$

which is typically of order one when we have a sizable K_A (so we have a large magnon gap $\Delta > \omega_L, \omega_R$). Here we have assumed $k_F \ll 1$ which is also required if we need the vortex-vortex interaction to be sizable for $L \gg 1$ (recall that here we have set the lattice spacing $a = 1$ for simplicity).

When $\omega_R = \omega_L = \Omega_0$ in the absence of magnetic field, the effective interaction can be simplified to

$$\begin{aligned} \mathcal{V} &= -\frac{\lambda^2 \mathcal{J}_A^2 \chi_\perp(\Omega_0)}{4\hbar} \left[(d_{1R}^\dagger + d_{1L})(d_{2R}^\dagger + d_{2L}) + (d_{2L}^\dagger + d_{2R})(d_{1L}^\dagger + d_{1R}) \right] + \text{h.c.} \\ &= \frac{\mathcal{J}_A^2 \chi_\perp(\Omega_0)}{2\hbar} (-\mathcal{X}_1 \mathcal{X}_2 + \mathcal{Y}_1 \mathcal{Y}_2), \end{aligned} \quad (\text{S18})$$

where we have rewritten the effective potential in terms of the collective coordinates of the vortices. Here we have focused on the case of $p = +1$, $\mathcal{N} = +1$. For polarity $p = \pm 1$ and topological charge $\mathcal{N} = \pm 1$, one can easily verify that the effective interaction between vortices is given by Eq. (10) in the main text.

(ii) Trajectories of the vortex

Here we discuss the trajectories of the vortex in the magnetic dot with the applied magnetic field and current. Following directly from the equation of motion for the vortex [Eq. (7) in the main text], we write down the following equation for the vortex trajectory:

$$\partial_t^2 \mathcal{Z}(t) - 2\omega_c i \partial_t \mathcal{Z}(t) + 2\gamma \partial_t \mathcal{Z}(t) + \Omega_0^2 \mathcal{Z}(t) = \mathcal{Z}_0 \Omega_0^2, \quad (\text{S19})$$

where $\mathcal{Z}(t) = \mathcal{R}_x(t) + i\mathcal{R}_y(t)$ represents the vortex position and $\mathcal{Z}_0 = 2\omega_c(u_y - iu_x)/\Omega_0^2$ is the stationary position of the vortex with the applied magnetic field and in-plane current. Assuming that the vortex is static at the disk center at time $t = 0$, the vortex trajectory is solve to be:

$$\frac{\mathcal{Z}(t)}{\mathcal{Z}_0(t)} = 1 - \frac{\Omega_+ e^{-i\Omega_- t} + \Omega_- e^{i\Omega_+ t}}{\Omega_+ + \Omega_-}, \quad (\text{S20})$$

where $\Omega_{\pm} = \sqrt{\Omega_0^2 + (\omega_c + i\gamma)^2} \pm (\omega_c + i\gamma)$. We show the trajectories of the vortex in Fig. S4 for different effective cyclotron frequencies (magnetic fields) and damping. Note that, in the absence of the damping $\gamma = 0$, the vortex trajectory is reduced to $\mathcal{Z}(t) = \mathcal{Z}_0[1 - (\omega_R e^{-i\omega_L t} + \omega_L e^{i\omega_R t})/2\Omega]$ as we discussed in the main text.

-
- [1] S. Bravyi, D. P. DiVincenzo, and D. Loss, Schrieffer–wolff transformation for quantum many-body systems, *Annals of physics* **326**, 2793 (2011).
 - [2] L. Trifunovic, F. L. Pedrocchi, and D. Loss, Long-distance entanglement of spin qubits via ferromagnet, *Phys. Rev. X* **3**, 041023 (2013).